



HAL
open science

Structural and magnetic properties of molecular beam epitaxy $(\text{MnSb}_2\text{Te}_4)_x(\text{Sb}_2\text{Te}_3)_{1-x}$ topological materials with exceedingly high Curie temperature

Candice R Forrester, Christophe Testelin, Kaushini Wickramasinghe, Ido Levy, Dominique Demaille, David Hrabovsky, Xiixin Ding, Lia Krusin-Elbaum, Gustavo E Lopez, Maria C Tamargo

► To cite this version:

Candice R Forrester, Christophe Testelin, Kaushini Wickramasinghe, Ido Levy, Dominique Demaille, et al.. Structural and magnetic properties of molecular beam epitaxy $(\text{MnSb}_2\text{Te}_4)_x(\text{Sb}_2\text{Te}_3)_{1-x}$ topological materials with exceedingly high Curie temperature. *APL Materials*, 2024, 12 (7), 10.1063/5.0195940 . hal-04734332

HAL Id: hal-04734332

<https://hal.science/hal-04734332v1>

Submitted on 14 Oct 2024

HAL is a multi-disciplinary open access archive for the deposit and dissemination of scientific research documents, whether they are published or not. The documents may come from teaching and research institutions in France or abroad, or from public or private research centers.








L'archive ouverte pluridisciplinaire **HAL**, est destinée au dépôt et à la diffusion de documents scientifiques de niveau recherche, publiés ou non, émanant des établissements d'enseignement et de recherche français ou étrangers, des laboratoires publics ou privés.



Distributed under a Creative Commons Attribution 4.0 International License

RESEARCH ARTICLE | JULY 12 2024

Structural and magnetic properties of molecular beam epitaxy $(\text{MnSb}_2\text{Te}_4)_x(\text{Sb}_2\text{Te}_3)_{1-x}$ topological materials with exceedingly high Curie temperature

Candice R. Forrester ; Christophe Testelin ; Kaushini Wickramasinghe; Ido Levy ; Dominique Demaille; David Hrabovsky ; Xiaxin Ding ; Lia Krusin-Elbaum; Gustavo E. Lopez ; Maria C. Tamargo 



APL Mater. 12, 071109 (2024)
<https://doi.org/10.1063/5.0195940>

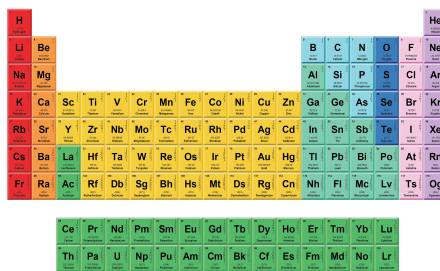


12 July 2024 19:26:51



THE MATERIALS SCIENCE MANUFACTURER®

Now Invent.™



American Elements
 Opens a World of Possibilities

...Now Invent!

www.americanelements.com

© 2024 American Elements is a U.S. Registered Trademark



Structural and magnetic properties of molecular beam epitaxy $(\text{MnSb}_2\text{Te}_4)_x(\text{Sb}_2\text{Te}_3)_{1-x}$ topological materials with exceedingly high Curie temperature

Cite as: APL Mater. 12, 071109 (2024); doi: 10.1063/5.0195940

Submitted: 4 January 2024 • Accepted: 28 June 2024 •

Published Online: 12 July 2024



View Online



Export Citation



CrossMark

Candice R. Forrester,^{1,2,3} Christophe Testelin,⁴ Kaushini Wickramasinghe,¹ Ido Levy,⁵ Dominique Demaille,⁴ David Hrabovsky,⁶ Xiaxin Ding,⁷ Lia Krusin-Elbaum,^{7,8} Gustavo E. Lopez,^{2,3} and Maria C. Tamargo^{1,2,8}

AFFILIATIONS

¹ Department of Chemistry, The City College of New York, New York, New York 10031, USA

² Ph.D Program in Chemistry, CUNY Graduate Center, New York, New York 10016, USA

³ Department of Chemistry, Lehman College, Bronx, New York 10468, USA

⁴ Institut des NanoScience de Paris, Sorbonne Université, CNRS, F-75005 Paris, France

⁵ Department of Physics, New York University, New York, New York 10003, USA

⁶ Sorbonne Université, MPBT Platform, 4 Place Jussieu, 75252 Paris, France

⁷ Department of Physics, The City College of New York, New York, New York 10031, USA

⁸ Ph.D Program in Physics, CUNY Graduate Center, New York, New York 10016, USA

ABSTRACT

Tuning the properties of magnetic topological materials is of interest to realize exotic physical phenomena, new quantum phases and quasi-particles, and topological spintronic devices. However, current topological materials exhibit Curie temperature (T_C) values far below those needed for practical applications. In recent years, significant progress has been made to control and optimize T_C , particularly through defect-engineering of these structures. Most recently, we reported T_C values up to 80 K for $(\text{MnSb}_2\text{Te}_4)_x(\text{Sb}_2\text{Te}_3)_{1-x}$ when $0.7 \leq x \leq 0.85$ by controlling the composition x and the Mn content in these structures during molecular beam epitaxy growth. In this study, we show further enhancement of the T_C , as high as 100 K, by maintaining high Mn content and reducing the growth rate from 0.9 nm/min to 0.5 nm/min. Derivative curves of the Hall resistance and the magnetization reveal the presence of two T_C components contributing to the overall value and suggest T_{C1} and T_{C2} have distinct origins: excess Mn in MnSb_2Te_4 septuple layers (SLs) and high Mn content in $\text{Sb}_{2-y}\text{Mn}_y\text{Te}_3$ quintuple layer (QL) alloys, respectively. To elucidate the mechanisms promoting higher T_C values in this system, we show evidence of enhanced structural disorder due to the excess Mn that occupies not only Sb sites but also Te sites, leading to the formation of a new crystal structure for these materials. Learning to control defects that enhance desired magnetic properties and understanding the mechanisms that promote high T_C in magnetic topological materials such as $(\text{Mn}_{1+y}\text{Sb}_{2-y}\text{Te}_4)_x(\text{Sb}_{2-y}\text{Mn}_y\text{Te}_3)_{1-x}$ is of great importance to achieve practical quantum devices.

© 2024 Author(s). All article content, except where otherwise noted, is licensed under a Creative Commons Attribution (CC BY) license (<https://creativecommons.org/licenses/by/4.0/>). <https://doi.org/10.1063/5.0195940>

INTRODUCTION

Three dimensional (3D) topological insulators (TIs) continue to gain attention for their unique properties, which are advantageous for novel electronic applications, including spintronics^{1,2} and quantum computing.^{3,4} 3D TIs, with molecular formulas V_2VI_3 , in which

the group V elements are Bi or Sb and the group VI elements are Se and Te, emerged as a new class of materials with inverted conduction and valence bands as a result of the strong spin-orbit coupling.^{5,6} This was first explored theoretically by Kane and Mele, who proposed a new classification scheme for the Z_2 topological invariant that distinguishes ordinary insulators from topological insulators.⁷

Due to the topological nature of these materials, qubits made from 3D TIs are expected to be robust to external perturbations and decoherence effects, hence fault tolerant.⁸ TIs are unique materials that are comprised of insulating (semiconducting) bulk interiors and conducting Dirac surface states in which the electrons are massless and move along the surface in a spin-locked helical direction and are protected by time reversal symmetry (TRS).^{6,7,9} Structurally, 3D TIs have a rhombohedral, R3m space group and self-assemble into quintuple layer (QL) units, held together via weak van der Waals forces.^{10–12}

The introduction of magnetic ions in TIs alters their band structure in fundamental ways. Magnetic topological insulators (MTIs) experience broken TRS due to spontaneous magnetization introduced by magnetic ions. The interaction between the surface states and the magnetic ions causes a gap to form at the Dirac point, which enables the observation of exotic physical phenomena, like the quantum anomalous Hall effect (QAHE), in these systems.¹³ Early work with Cr doped (Bi,Sb)₂Te₃^{14,15} demonstrated QAHE in such 2D systems, where electrons can exhibit dissipationless transport in the absence of a magnetic field, leading to the discovery of a new class of materials whose strong spin-orbit coupling suppresses electron backscattering. This makes them highly efficient in spin-to-charge conversions.¹⁵ Recently, a new class of MTIs has been discovered in which the addition of a magnetic ion results in a new compound of the generalized form: MV₂VI₄, where M is a transition-metal or rare-earth element, the group V elements are Bi or Sb, and the group VI elements are Te or Se.^{12,16–18} In the case of MnSb₂Te₄, recent studies propose that the materials are MTIs,¹⁹ while other research suggests the presence of Mn results in a Weyl semimetal.^{20–22} Such topologically nontrivial phases have enabled the demonstration of chiral Weyl fermions²³ and may also lead to exotic electronic, optical, and magnetic properties.²⁴ In these materials, the incorporation of Mn modifies the crystal structure into a septuple layer (SL) unit structure that has a Mn layer in the center of the unit cell.

While bulk MnBi₂Te₄ and MnSb₂Te₄ are both intrinsically antiferromagnetic, a single SL is ferromagnetic (FM) with spins aligned out of the plane.^{24,25} Several approaches have been used to induce FM coupling between SLs, including separating individual FM SLs with non-magnetic QLs,²⁵ having an odd number of SLs,²⁶ or introducing excess Mn, in the form of Mn antisites, into the all-SL structure.^{16,19,27} For MnBi₂Te₄, separating FM SLs with non-magnetic Bi₂Te₃ QLs not only demonstrated the QAHE but also resulted in a material with a Curie temperature (T_C) of about 15 K.^{17,25} In the case of excess Mn in MnSb₂Te₄, Wimmer et al. observed a T_C of 50 K,¹⁹ and most recently, our group reported T_C values of 80 K in structures of (MnSb₂Te₄)_x(Sb₂Te₃)_{1-x}, when $x = 0.7–0.85$.²⁸ Such T_C values are the highest reported for these material systems.

The addition of Mn during growth, both by bulk or epitaxial techniques, results in the formation of self-assembled stacks of varying ratios of QL and SL depending on the relative Mn to Sb ratios used during growth.^{12,27,29} Structurally, Mn ions can be incorporated into a QL TI host crystal, either substituting for one of the constituent atoms in the QL or as a structural element forming the new SL crystal structure.^{17,18,27,30} Both types of substitutions have significant effects on the properties of the final structure, and the mechanisms promoting the observed high T_C are not well known. Many have proposed that the presence of the Mn antisites

in the SL can produce increased T_C values,^{16,19} while others have shown that alloy formation with transition metal ions (TMs) such as Sb_{2-y}TM_yTe₃ can also yield very high T_C.^{31–33}

In this work, we report on self-assembled (MnSb₂Te₄)_x(Sb₂Te₃)_{1-x} structures grown by molecular beam epitaxy (MBE), with exceptionally high T_C values of more than 100 K, by further tuning the growth parameters, in particular by reducing the growth rate. These values are by far the highest T_C observed for this material system. Temperature dependent Hall resistance (R_{xy}) and magnetization measurements both reveal the high T_C. Other characterization techniques such as x-ray diffraction rocking curves and energy-dispersive x-ray spectroscopy (EDS) were used to investigate the structural properties. We observed that samples grown at slow growth rates have more disorder, in the form of excess Mn possibly occupying both Sb and Te sites. We propose that, for high Mn content samples, the Mn is incorporated both in the SLs and the QLs and propose the formation of a new composite material: (Mn_{1+y}Sb_{2-y}Te₄)_x(Sb_{2-y}Mn_yTe₃)_{1-x} that gives rise to the exceedingly high T_C values. Although the specific topological nature of the MnSb₂Te₄ SL material is not well established, transition metals containing QL alloys, such as Sb_{2-y}TM_yTe₃, are anticipated to be MTIs,^{14,34,35} rendering these composite materials extremely interesting both from their high T_C values as well as their potential non-trivial topology. Therefore, while this paper does not address the topological nature of our materials, learning to tune the magnetic properties of these materials to achieve higher T_C values can bring us closer to the design of practical spintronic and quantum devices.

EXPERIMENTAL DETAILS

All (MnSb₂Te₄)_x(Sb₂Te₃)_{1-x} structures were grown by MBE on (0001) c-plane sapphire substrates in a Riber 2300P system under ultra-high vacuum conditions (3–5 × 10⁻¹⁰ Torr) using a modified MBE growth procedure developed by our group.²⁹ The MBE is equipped with reflection high-energy electron diffraction (RHEED) to monitor surface quality of the samples as they grow.

Before the growth of (MnSb₂Te₄)_x(Sb₂Te₃)_{1-x}, the epi-ready sapphire substrates are baked at 670 °C for 1 h to remove any impurities on the sapphire surface. Fluxes for 6N antimony (Sb) with a Riber double zone cell and single zone Knudsen cells for 6N tellurium (Te) and 5N8 manganese (Mn) were measured by the beam equivalent pressure (BEP) obtained by a gauge placed in the substrate position. Self-assembled stacks of Sb₂Te₃ quintuple layers (QLs) and MnSb₂Te₄ septuple layers (SLs), of the formula (Sb₂Te₃)_{1-x}(MnSb₂Te₄)_x, were grown by controlling the ratio of the Mn to Sb fluxes during growth. The samples were grown with varying Mn BEP ratios, defined as BEP_{Mn}/(BEP_{Mn}+BEP_{Sb}), to control the (MnSb₂Te₄)_x(Sb₂Te₃)_{1-x} composition (i.e., the value of x) and under excess Te, with a Sb:Te ratio of 1:20. Previously, we showed the ability to grow structures of (MnSb₂Te₄)_x(Sb₂Te₃)_{1-x} in the entire composition range ($x = 0$ to $x = 1$), where x is the fraction of MnSb₂Te₄ SLs in the structure.

Two growth rate ranges were used: a fast growth rate of 0.9–1.0 nm/min and a slow growth rate of ~0.4–0.5 nm/min. The two growth rates were obtained by adjusting the Sb flux. Most of the slow growth rate samples were grown with a Mn BEP ratio of 0.09, which led to the highest T_C values for the fast growth rate samples.²⁸ For the

growth, the substrate temperature (T_{sub}) was first raised to $\sim 200^\circ\text{C}$, where the Sb and Te shutters were opened to grow a low temperature buffer (LTB) layer. The Sb_2Te_3 LTB was grown for 8–10 min until reconstruction of the RHEED was observed, indicating crystalline Sb_2Te_3 layer formation. The T_{sub} was then raised to 265°C , and the Mn shutter was opened to commence the growth of the desired layer of $(\text{MnSb}_2\text{Te}_4)_x(\text{Sb}_2\text{Te}_3)_{1-x}$. After 15 min of growth, the Sb and Mn shutters are closed, and the T_{sub} is raised to 300°C and held at this temperature for 15 min (15 min annealing). After the 15 min annealing, the T_{sub} is set back to the original growth temperature of 265°C . There, the Mn and Sb shutters are opened again, and the remaining $(\text{MnSb}_2\text{Te}_4)_x(\text{Sb}_2\text{Te}_3)_{1-x}$ thin film is grown for 1–2 h.²⁹

After growth, samples were characterized by various techniques, including atomic force microscopy (AFM) using a Bruker Dimension FastScan AFM with a FastScan-A silicon probe and high-resolution x-ray diffraction (HR-XRD) analysis using a Bruker D8 Discover diffractometer with a da Vinci configuration and a Cu $\text{K}\alpha 1$ (1.5418 Å) source. For further analysis, the (0012) x-ray rocking curves were measured using a crystal analyzer. Transport measurements were performed in the van der Pauw geometry with indium contacts using a 14 T Quantum Design physical property measurement system (PPMS) in a 1 mTorr (at low temperature) of He gas or in a Lakeshore 7600 electromagnetic system. Magnetization measurements of the samples were made using a superconducting quantum interference device (SQUID, MPMS3 from Quantum Design). Energy-dispersive x-ray spectroscopy (EDS) measurements were made in a Zeiss Supra 40 with a compact 30 mm Bruker detector.

RESULTS AND DISCUSSION

Previous work by our group showed that the highest Curie temperature values for these materials, as high as 80 K, were achieved in $(\text{MnSb}_2\text{Te}_4)_x(\text{Sb}_2\text{Te}_3)_{1-x}$ for values of x between 0.7 and 0.85 (70%–85% SLs).²⁸ In that work, the highest T_C values were obtained with a Mn BEP ratio of about 0.09, a growth temperature of 265°C , and a 15 min pre-annealing step. Typical growth rates for those materials were 0.9–1.0 nm/min, referred to in the remainder of this paper as “fast growth rates”. Details of the growth can be found in the supplementary material in Ref. 29. In this work, we will show that by reducing the growth rate to ~ 0.4 – 0.5 nm/min (“slow growth rates”), the Curie temperature has increased further to values above 100 K. We first examine the structural and magnetic properties of these new slow growth rate materials to better understand the reason for the high T_C values in these structures.

Structural and electrical properties of $(\text{MnSb}_2\text{Te}_4)_x(\text{Sb}_2\text{Te}_3)_{1-x}$ with $x \geq 0.7$ grown with slow growth rate

During the growth by molecular beam epitaxy, the surface was monitored *in situ* using reflection high energy electron diffraction (RHEED), where the observed patterns indicate the crystalline and surface quality of the material as it grows. As in the case of the fast growth rate samples reported in Ref. 28, we observed streaky RHEED patterns for the slow growth rate samples, signifying good crystallinity and smooth surfaces. AFM images of the surfaces

also indicate smooth surfaces, typical of the Sb_2Te_3 based materials, and their quality is unchanged with the changing growth rates (see supplementary material, Figs. S1 and S2).

In this work, we aimed to grow samples at slower growth rates with compositions $x \geq 0.7$, which are the compositions that previously yielded the higher T_C values. The samples were characterized using high resolution x-ray diffraction (XRD) 2θ - ω scans to determine their composition x (or %SLs, as described in Refs. 28 and 29). The value of x was calculated using Vegard's law by measuring the shift in the (0015) Sb_2Te_3 peak as it transforms into the (0021) MnSb_2Te_4 peak. The peak position indicates the average composition of SLs and QLs in the structure. A comparison of the XRD calculations with high resolution transmission electron microscopy (HR-TEM) cross sections confirmed the accuracy of the XRD method. Full details can be found in Levy *et al.*²⁹ Figure 1(a) summarizes the results of the slow growth rate samples grown, shown in blue circles, compared to previously reported compositions (red circles) for the fast growth rate samples.²⁸ As seen in Fig. 1(a), for the same Mn BEP ratios, slightly lower compositions are obtained for the samples grown at the slow growth rates; furthermore, we were unable to achieve 100% SL (or compositions of $x = 1.0$) using slow growth rates. Figure 1(b) compares the 2θ - ω scans of two samples having similar thicknesses of 53 and 66 nm, one grown at fast growth rates (red) and another grown at slow growth rates (blue), respectively. Based on the position of the (0021) peak in these samples, the calculated compositions are $x = 0.72$ and $x = 0.80$, respectively. To better assess the crystalline quality, a more sensitive study using x-ray rocking curves was performed to compare the quality of the fast and slow growth rate samples. Based on the full-width-half-maximum (FWHM) of the rocking curves shown in Fig. 1(c) (the slow growth rate sample has a FWHM of 1.59° , while for the fast growth rate sample, it is 0.99°), we conclude that the slow growth rate produces material with similar composition but a higher degree of crystalline disorder. Finally, since the Mn ions behave as electrical dopants in these materials, we also explored the impact of the slow growth rate on the electrical properties of these samples.

Hall effect measurements at high magnetic fields were performed for some of the samples grown at slow growth rates and compared to previously reported values for samples grown at fast growth rates.²⁸ As seen in Fig. 1(d), the slow growth rate samples (blue squares) follow the same dotted line trend as the fast growth rate samples (red squares), indicating that the slow growth rate does not have a significant effect on the samples' carrier density. Our data²⁸ show that incorporation of Mn in Sb_2Te_3 results in very high carrier densities, of the order of 10^{20} – 10^{21} cm^{-3} , which may interfere with accessing the non-trivial topological surface states.²⁸ Nonetheless, the carrier density quickly decreases for materials with a large SL composition, opening the perspective of significantly reducing the carrier doping in MnSb_2Te_4 . Moreover, partial substitution of Sb with Bi has been shown by others to reduce carrier densities, making it possible to reach low doping and preserve the non-trivial nature of the material.^{36–39}

Magnetic properties of $(\text{MnSb}_2\text{Te}_4)_x(\text{Sb}_2\text{Te}_3)_{1-x}$ with $x \geq 0.7$ grown at slower growth rate

Field dependent Hall resistance was measured at 10 K for all the samples grown at slow growth rates. As was the case for

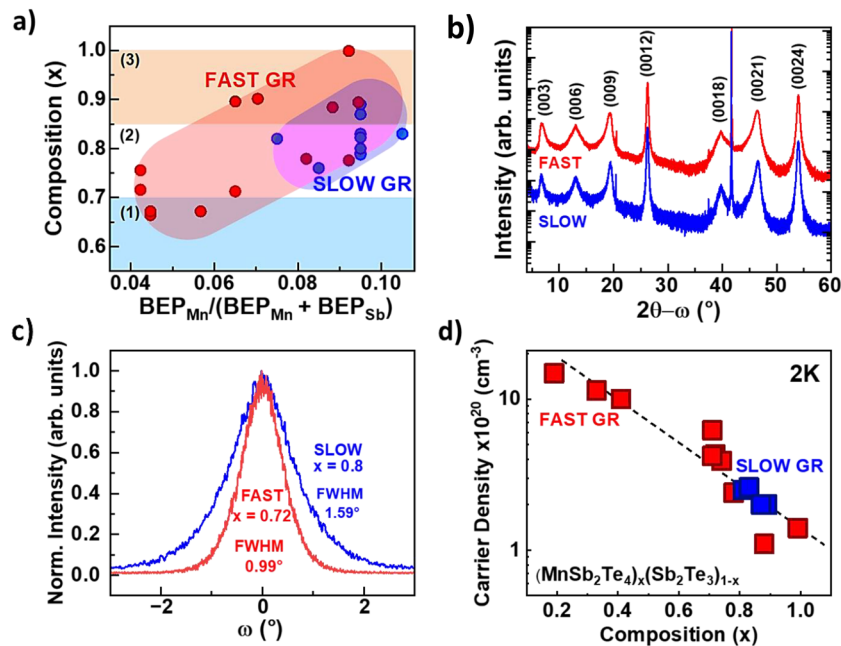


FIG. 1. Structural and electrical properties of $(\text{MnSb}_2\text{Te}_4)_x(\text{Sb}_2\text{Te}_3)_{1-x}$ structures grown at slow growth rates. (a) Fraction (x) of MnSb_2Te_4 as a function of Mn BEP ratio for samples grown with slow growth rates (blue points) superimposed on the corresponding data previously obtained for samples grown at a fast growth rate (red points). Based on the fraction (x), three composition regions are defined:²⁸ region 1, where $x < 0.7$ (light blue), region 2, where $0.7 \leq x \leq 0.85$ (white), and region 3, where $x > 0.85$ (orange). Blue and red oval shaded regions are used to highlight the relationship between the Mn BEP ratio and the fraction of MnSb_2Te_4 . (b) 2θ - ω x-ray diffraction scans for two samples of $(\text{MnSb}_2\text{Te}_4)_x(\text{Sb}_2\text{Te}_3)_{1-x}$, one grown at a slow growth rate (blue trace) and the other at a fast growth rate. (c) Comparison of (0012) rocking curves of slow growth rate (blue) and fast growth rate (red) samples. The broader (0012) peak measured for the slow growth rate sample indicates more disorder. (d) Carrier density as a function of fraction (x) of MnSb_2Te_4 for fast (red squares) and slow (blue squares) growth rate samples. Higher fractions of MnSb_2Te_4 have lower carrier densities. Reducing the growth rate did not affect the carrier density for samples with the same SL fraction.

the fast growth rate samples,²⁸ the plots all show typical hysteresis behavior, signifying the ferromagnetic (FM) nature of all the samples investigated. Ferromagnetic behavior was also observed in magnetization measurements made using a SQUID magnetometer (see supplementary material, Fig. S3). Figure 2 illustrates the temperature dependent Hall resistance and magnetization measurements of the slow growth rate samples for samples with a composition of $0.7 < x < 0.85$. This composition range, which we previously called Region 2,²⁸ produced the highest T_C values (as high as 80 K) for fast growth rate samples. Figure 2(a) compares the normalized temperature dependent Hall resistance for two samples with similar compositions, one grown at a slow growth rate and the other at a fast growth rate. The value at which the Hall resistance goes to zero is taken as the value of the T_C . According to Fig. 2(a), the fast growth rate sample has a T_C of ~ 80 K, as reported in Ref. 28, while the slow growth rate sample has a value of ~ 100 K, 25% higher than our previously reported value and the highest T_C value reported to date for these materials systems. This value is confirmed by magnetization measurement in a SQUID magnetometer, where the magnetic moment (M) was measured as a function of temperature at 200G, as shown in Fig. 2(b). A T_C value of ~ 100 K was observed from the magnetization measurement study, in agreement with the Hall resistance data. The inset in Fig. 2(b) shows a magnified view of the

temperature dependent Hall resistance measurement in Fig. 2(a) for the slow growth rate sample, which shows excellent agreement between the two measurements.

To clearly establish the value of the T_C , derivative curves were plotted for both the Hall resistance (R_{xy}) and magnetization (M) data. In our earlier work, we showed that the derivative curves of the temperature dependent R_{xy} gave evidence of two Curie temperatures, a low T_C of about 20 K and a high T_C of 80 K for the fast growth samples. Similarly, two distinct T_C components could also be seen from the derivative plots of the slow growth rate samples shown here: a low T_C , T_{C1} , at ~ 20 K, and a second higher T_C , T_{C2} , with a broad, weaker signal reaching a value greater than 100 K; this is shown in Fig. 2(c). Evidence for the two T_C components is also obtained from the derivative plot of the magnetization data, shown in Fig. 2(d), with T_C values in excellent agreement with the Hall resistance data. Finally, further evidence of the very high T_{C2} value for the slow growth rate samples is obtained from the field dependent R_{xy} plots, which show hysteresis loops that persist up to 100 K, as shown in Fig. 2(e). Field dependent magnetization measurements were also made, as shown in Fig. 2(f). Hysteresis loops were evident up to about 80 K (solid line), demonstrating the presence of a high T_C , although not as high as that measured from R_{xy} or as expected from the magnetization derivative plot. We believe that

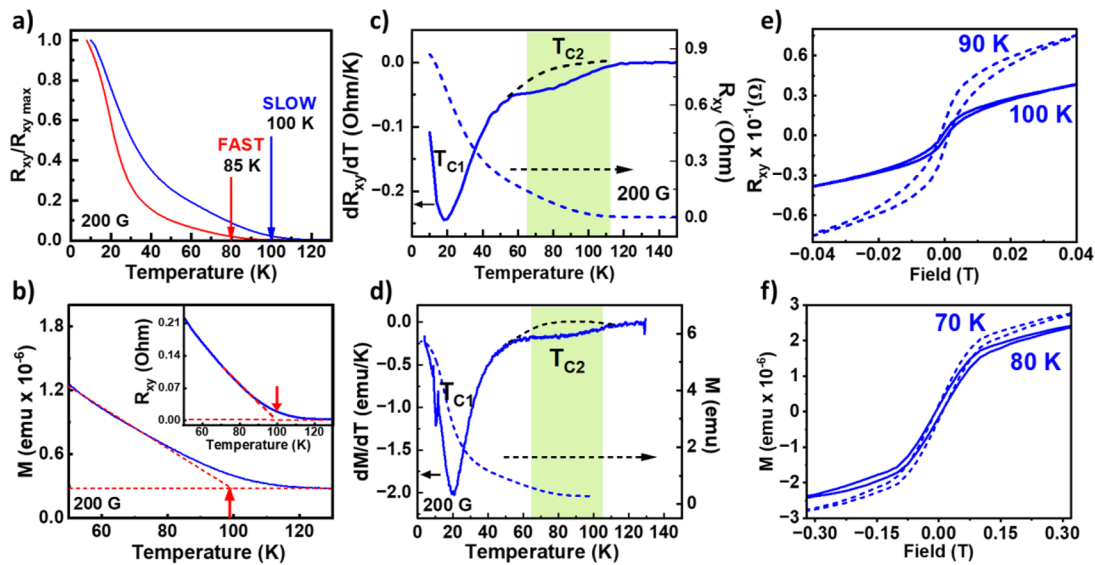


FIG. 2. Magnetic properties of $(\text{MnSb}_2\text{Te}_4)_x(\text{Sb}_2\text{Te}_3)_{1-x}$ structures with $0.7 \leq x \leq 0.85$ (Region 2). (a) Normalized temperature dependent Hall resistance (R_{xy}) at 200 G of two samples, one grown at fast growth rates (red trace) and the other at slow growth rates (blue trace). The slow growth rate sample exhibited a T_C of about 100 K. (b) Temperature dependent magnetization measurements for the slow growth rate sample shown in (a). Good agreement is seen between the magnetization measurement and the Hall resistance measurement (inset). (c) Superimposed plot of temperature dependent Hall resistance R_{xy} (dashed) and its derivative curve (solid) for a sample grown at a slow growth rate. Two transitions are seen, indicating two T_C components: one at ~ 20 K and another reaching as high as 100 K. (d) Superimposed plot of temperature dependent magnetic moment (M) (dashed) and its derivative curve (solid) for the sample grown with a slow growth rate. Two T_C components are seen, as in (c). (e) Field dependent Hall resistance measurement for the slow growth rate sample with $x = 0.83$, showing hysteresis up to 100 K. (f) Field dependent magnetic moment (M) of the samples of (e), showing hysteresis up to 80 K.

the suppression of the hysteresis loop at a lower temperature in the magnetization plots is probably due to the lower sensitivity of the magnetization probe.

We also investigated samples with composition $x > 0.85$, which we had previously identified as Region 3.²⁸ At the fast growth rates, the samples in Region 3 had lower T_C values than the samples in Region 2, with T_C on the order of 40 K. An example of this is shown by the normalized temperature dependent Hall resistance data given by the red trace in Fig. 3(a). The figure also shows the result for a sample grown at a slow growth rate (blue trace). The temperature dependent R_{xy} plot suggests a high T_C component (T_{C2}) of ~ 75 K for the slow growth rate sample, significantly higher than the 40 K observed for the fast growth rate sample. Derivative curves of the R_{xy} plots of the slow growth rate sample [Fig. 3(b)] show evidence of two T_C components, and the field dependent R_{xy} [Fig. 3(c)] shows a T_{C2} as high as 75 K (solid line), suggesting a similar effect on the T_C by the reduced growth rates in Region 3 samples.

Control of the bulk carrier density and transport properties of these materials is of utmost importance to exploit the topological surface features for practical applications. Furthermore, the relationship between the carrier density and the T_C may be examined to provide some insight as to the type of magnetic interactions at play in these materials. In Fig. 3(d), we plot the T_{C2} of samples with $x > 0.7$ (Regions 2 and 3) as a function of their carrier concentration for samples grown at both fast and slow growth rates. No apparent correlation between T_C and carrier density is observed. The two principal mechanisms used to describe ferromagnetic

interactions in magnetic topological materials are the Ruderman–Kittel–Kasuya–Yosida (RKKY) mechanism and the Van Vleck mechanism.^{40–43} While RKKY predicts that enhanced magnetic coupling is dependent on carrier density, the Van Vleck mechanism predicts that ferromagnetic behavior and T_C are not carrier mediated.^{18,44,45} Our results shown in 3d, in which the slow GR samples with similar x values yielded comparable carrier densities but significantly higher T_C values, suggest Van Vleck or long-range magnetic interaction mechanisms more closely describe the properties observed in these complex materials. However, a more in-depth investigation is needed to establish the types of magnetic interactions that lead to such high T_C values in these complex materials.

Mn content of $(\text{MnSb}_2\text{Te}_4)_x(\text{Sb}_2\text{Te}_3)_{1-x}$ structures as a function of composition and growth rate: Correlation with T_C values

Excess Mn has been previously identified as a likely factor in determining the T_C value of these materials.^{16,19} To explore this, we investigated the effects of growth rate on the elemental concentration of the $(\text{MnSb}_2\text{Te}_4)_x(\text{Sb}_2\text{Te}_3)_{1-x}$ samples using energy dispersive x-ray spectroscopy (EDS). The elemental contributions of Mn, Sb, and Te were plotted as a function of composition (x) in the structure for a set of samples grown at fast and slow growth rates.

The results are plotted in Figs. 4(a) and 4(b). The solid black lines represent calculated values expected for stoichiometric

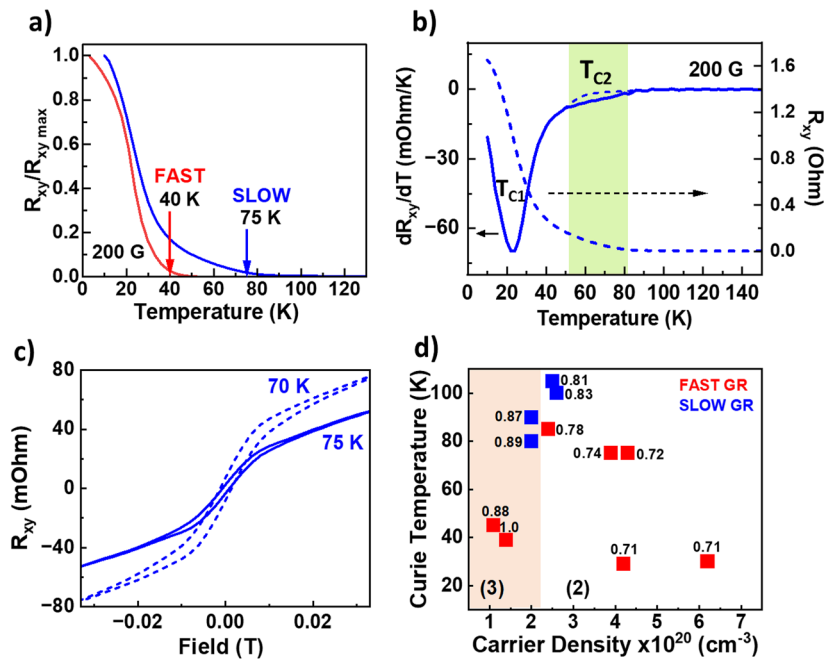


FIG. 3. Magnetic properties of $(\text{MnSb}_2\text{Te}_4)_x(\text{Sb}_2\text{Te}_3)_{1-x}$ structures with $x \geq 0.85$ (Region 3). (a) Normalized temperature dependent Hall resistance (R_{xy}) taken at 200G for two samples of region 3, one grown with fast growth rates (red) and another grown with slow growth rates (blue). The slow growth rate sample exhibited a T_C of about 75 K. (b) Superimposed plot of temperature dependent Hall resistance (dashed) and its derivative curve (solid) for the sample grown at a slow growth rate. Two T_C components are seen: one at 20 K and a second, broader one reaching as high as 80 K. (c) Field dependent Hall resistance (R_{xy}) for the slow growth rate sample, showing hysteresis up to 75 K. (d) Curie temperature T_C plotted as a function of carrier density for samples with $x \geq 0.7$ (Regions 2 and 3) grown at fast (red points) and slow (blue points) growth rates. The value of x for each sample is indicated for each point. No correlation between T_C and carrier density is observed.

$(\text{MnSb}_2\text{Te}_4)_x(\text{Sb}_2\text{Te}_3)_{1-x}$ layers, while the red data points represent the EDS data for a set of fast growth rate samples²⁸ and the blue points represent the slow growth rate samples of this study. At low SL concentrations, where $x \leq 0.7$, the data for fast growth rate samples largely follow the predicted curves for stoichiometric samples. However, when $x > 0.7$, the points begin to deviate significantly from the stoichiometric lines, showing increasing Mn content, well in

excess of the stoichiometric amounts, and a corresponding decrease in Sb content, consistent with most of the excess Mn occupying Sb sites.

In the case of the slow growth rate samples, which all lie in this composition range of $x \geq 0.7$, the excess Mn in the samples is even greater, and the Sb concentration is lower than for the fast growth rate samples. Furthermore, for the samples with a slow growth rate,

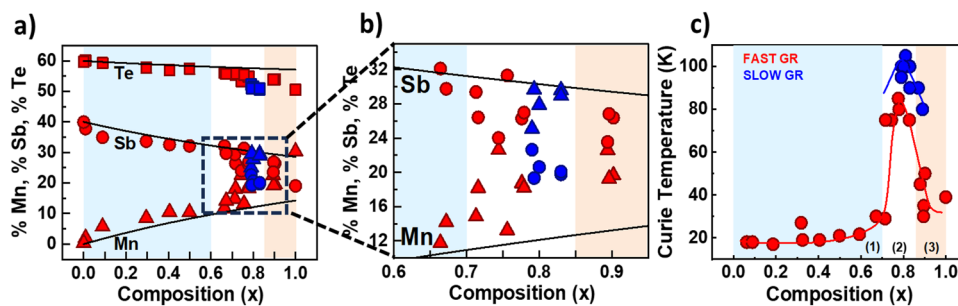


FIG. 4. Structural factors influencing the Curie temperature. (a) EDS characterization of a selection of samples grown at a fast growth rate (red) and slow growth rate (blue); solid lines represent composition for stoichiometric $(\text{MnSb}_2\text{Te}_4)_x(\text{Sb}_2\text{Te}_3)_{1-x}$. Site mixing between Mn and Sb is evident for fast growth rate samples with x above 0.7. Samples grown at a slower growth rate show a further increase in site mixing between Mn and Sb, as well as between Mn and Te atoms. (b) A magnified view of the Sb and Mn EDS data for samples with $x \geq 0.7$. (c) Curie temperature as a function of composition x of $(\text{MnSb}_2\text{Te}_4)_x(\text{Sb}_2\text{Te}_3)_{1-x}$. Slow growth rate samples (blue points) consistently exhibit higher T_C values for the same value of x .

12 July 2024 19:26:51

some reduction in the Te concentration is also seen, suggesting that Mn is also substituting for Te atoms in the crystal. This means that the greater disorder introduced by the slower growth rates is related to more excess Mn occupying Sb sites and sometimes Te sites, as indicated by the EDS data. Figure 4(b) shows a magnified view of the region of interest [the dashed square in Fig. 4(a)] to illustrate this phenomenon more clearly. It is evident that the Mn fractions (blue triangles) are much higher than the stoichiometric Mn values, while the Sb fractions (blue circles) are much lower than the stoichiometric Sb values. Therefore, we conclude that the excess Mn in the crystal is greatly enhanced by the slow growth rates. It is important to note that it is within this composition range that we see evidence for the high T_C in the samples. This can be seen in Fig. 4(c), which shows the relationship between T_C and composition x for fast growth rate samples (in red) and slow growth rate samples (in blue). The data show that the high T_C for the fast growth rate samples and the even higher T_C for the slow growth rate samples occur when $0.7 \leq x \leq 0.85$, the same region where the excess Mn is present. A similar relationship between the T_C and Mn fractions is also observed (see supplementary material Fig. S4). Our results point to two factors that are essential for the observation of a high T_C : (1) a large excess Mn substituting for the Sb, i.e., Mn_{Sb} antisites, and (2) a sufficient fraction of QLs in the structure, i.e., $x < 1$.

The EDS results show that at the reduced growth rate, the incorporation of Mn into the crystal structure is enhanced for the same Mn flux ratio used during growth. This can be understood if we consider that at the typical MBE growth temperatures, Sb desorption (and possibly also Te desorption) and its subsequent substitution by Mn may be favored when growth takes place more slowly. In addition, investigations of our samples' magnetic properties give evidence for two different magnetic interactions giving rise to the two different T_C values. Similarly to what we previously proposed,²⁸ the excess Mn obtained at the slower growth rates of this study incorporates both in the SLs, giving rise to more Mn-rich SLs of the form $Mn_{1+y}Sb_{2-y}Te_4$ and to QL-alloys of the form $Sb_{2-y}Mn_yTe_3$ with very high y values (see supplementary material Fig. S5). These QL alloys have been predicted to have a high T_C ³³ and may lead to the observed

exceedingly high T_{C2} values of up to 100 K. To further support this proposal, we estimate the values of y in our samples using the measured EDS elemental compositions and assume for simplicity, that the excess Mn is incorporated equally into the SLs and QLs. Furthermore, we used the Sb fraction (X_{Sb}) measured by EDS rather than the Mn fraction (X_{Mn}). This was performed to reduce errors arising from possible Mn incorporation into crystalline sites other than Sb sites (Te-antisites or others). The data for both the fast growth rate samples of Ref. 28 and the new slow growth rate samples of this study are plotted in Fig. 5(a), using the equation

$$y = 2 - \chi_{sb}(5 + 2x).$$

The error in the value of y is estimated to be ± 0.035 , making the lowest data point, with a T_C of 25 K, have $y \sim 0$, and suggesting that the observed T_C for this sample is likely due to the $Mn_{1+y}Sb_{2-y}Te_4$ SLs in the structure. A very close agreement between the proposed T_C values³³ and our experimental results is observed, supporting our proposed mechanism for the high T_C values. Our results suggest that samples with $T_{C2} \sim 100$ K contain QLs with compositions of $Sb_{1.4}Mn_{0.6}Te_3$.

Figure 5(b) illustrates the proposed structure for samples with $x \geq 0.7$ that contain a mixture of QLs and SLs. To obtain these high x values, growth by MBE requires the use of very large Mn BEP ratios, and as shown by the EDS results, there is a large excess of Mn in the crystal, which is even greater for the slow growth rate samples. In these samples, our data suggest that excess Mn is incorporated into the QL to form $Sb_{2-y}Mn_yTe_3$ alloys, a material that is predicted to be ferromagnetic with very high T_C values.³³ The Mn content (y) in the QLs is largest when the samples are grown at slow growth rates, leading to the observed exceedingly high T_{C2} . The SLs also contain excess Mn, forming $Mn_{1+y}Sb_{2-y}Te_4$, which have been shown to yield T_C values of 20–50 K.^{16,19,28} The three frames of Fig. 5(b) describe the magnetic properties of these structures as the temperature increases. Below T_{C1} , the SLs of composition $Mn_{1+y}Sb_{2-y}Te_4$ and QLs of composition $Sb_{2-y}Mn_yTe_3$ are both magnetized, and the structure exhibits strong FM behavior.

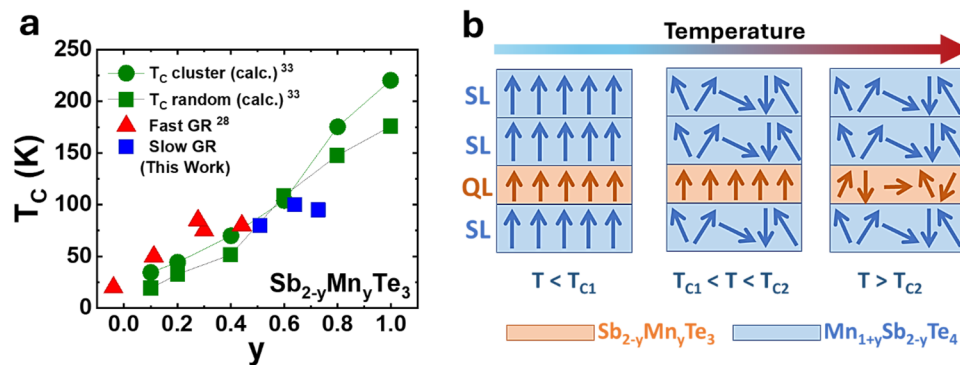


FIG. 5. Considerations for the proposed origin of the high T_C values. (a) T_C as a function of y , where y is the Mn fraction in the $Sb_{2-y}Mn_yTe_3$ alloy. Experimental data for slow growth samples (this study, blue squares) are compared to predicted data³³ and to fast growth rate data²⁸ (red triangles). (b) Schematic illustrating the proposed origin of the two T_C components in $(Mn_{1+y}Sb_{2-y}Te_4)_x(Sb_{2-y}Mn_yTe_3)_{1-x}$ samples with $x \geq 0.7$. Two distinct ferromagnetic materials, $Mn_{1+y}Sb_{2-y}Te_4$ (blue, SLs) and $Mn_ySb_{2-y}Te_3$ (red, QLs), give rise to two distinct T_C values, which can be observed as the temperature of the material increases.

Above the T_{C1} but below T_{C2} , the spins in the SLs are randomized, and only the spins in the QL alloys remain aligned, producing a weaker magnetization due to the relatively low fraction of QLs in the structure but leading to the high T_{C2} that we observe in the R_{xy} and M curves. Finally, above T_{C2} , all spins are randomized, and the material is paramagnetic. As stated earlier, our results suggest that high Mn content $Sb_{2-y}Mn_yTe_3$ QLs are responsible for the high T_{C2} values in our materials. Such high Mn content $Sb_{2-y}Mn_yTe_3$ alloys have not been previously realized experimentally and are likely formed here in our experiments due to the far from equilibrium MBE growth conditions. Further structural analysis would be helpful to fully ascertain the formation of this magnetic QL structure.

CONCLUSIONS

We have shown that by reducing the growth rate during MBE growth, the highest T_C values for $(MnSb_2Te_4)_x(Sb_2Te_3)_{1-x}$ structures reported to date, as high as 100 K, were achieved. These values are much higher than those reported by others^{16,19} and significantly higher than those recently reported by us²⁸ for samples grown at faster growth rates. The values were measured by both Hall resistance and SQUID magnetization measurements, yielding similar results. As in the fast growth rate samples previously reported, the results indicated the presence of two T_C components that we attribute to the two types of layers (SLs and QLs), both of which are ferromagnetic and have different T_C values. Structurally, no significant difference was apparent between samples grown at fast or slow growth rates. Only in the (0012) rocking curves did we see evidence of more disorder at the slow growth rates. Using EDS, we identified one important type of disorder that is present in these structures in the form of substitutional Mn, which is enhanced by the slow growth rates. The elemental composition of these structures showed evidence of a significant excess of Mn, likely in the form of Mn:Sb and some Mn:Te intermixing in both the SLs and the QLs.

The enhanced Mn content at slower growth rates is understood by recognizing that, due to the higher volatility of Sb (and Te), there is a greater probability for Sb (and Te) desorption when using slower growth rates, which increases the likelihood of Mn incorporation in Sb sites and even in Te sites. The increased Mn content results in a higher T_C for samples grown with the same Mn BEP ratio. We propose that significant incorporation of Mn is converting the Sb_2Te_3 QL into $Sb_{2-y}Mn_yTe_3$ alloys, which have been predicted to have very high T_C values. We thus propose a new crystal composition for our materials: $(Mn_{1+y}Sb_{2-y}Te_4)_x(Sb_{2-y}Mn_yTe_3)_{1-x}$. We illustrated the concept of two T_C components in our structures, where T_{C1} originates from the Mn-rich $Mn_{1+y}Sb_{2-y}Te_4$ SLs while T_{C2} originates from the Mn-rich $Sb_{2-y}Mn_yTe_3$ QLs. Finally, preliminary results that show no correlation between the carrier density and the high T_C suggest that the magnetic interactions are not carrier mediated, and long-range magnetic interactions are more likely at play in these materials. Although carrier density does not influence the high T_C values, adding Bi to these structures may lower the carrier density, making the surface states and topological features more accessible.

Our investigations provide evidence for a novel hybrid structure that is comprised of two types of magnetic topological materials: $Mn_{1+y}Sb_{2-y}Te_4$ and $Sb_{2-y}Mn_yTe_3$. The results also suggest that we have succeeded in forming a very high Mn content $Sb_{2-y}Mn_yTe_3$

alloy, which has not been experimentally demonstrated before. We also propose that, based on theoretical predictions about this material, the $Sb_{2-y}Mn_yTe_3$ is likely responsible for the very high T_{C2} (>100 K). Although in this study we have not ascertained the topological nature of these novel materials, the possibility of proximity effects affecting the overall nontrivial topology and magnetism of these composite structures renders these materials most interesting as potential contenders for new quantum devices. Our results suggest a pathway to magnetic topological materials with even higher T_C values and bring us closer to practical applications.

SUPPLEMENTARY MATERIAL

The supplementary material contains surface and cross-sectional characterization results of $(MnSb_2Te_4)_x(Sb_2Te_3)_{1-x}$ samples using reflection high energy electron diffraction (RHEED) and atomic force microscopy (AFM) as well as scanning transmission electron microscopy (STEM). It also contains field dependent magnetization and Hall resistance measurements for slow growth rate samples with $x \geq 0.7$, the relationship between Mn concentration (χ_{Mn}) of $(Mn_{1+y}Sb_{2-y}Te_4)_x(Sb_{2-y}Mn_yTe_3)_{1-x}$ materials and their Curie temperature, and a schematic illustrating the Mn incorporation sites in the $Sb_{2-y}Mn_yTe_3$ QLs and $Mn_{1+y}Sb_{2-y}Te_4$ SLs.

ACKNOWLEDGMENTS

This work was supported by NSF Grant No. DMR-2011738 (NSF MRSEC PAQM) and NSF Grant No. HRD-2112550 (Phase II CREST IDEALS). This work was also supported by Project No. DYN-TOP ANR-22-CE30-0026-01. The authors would like to acknowledge the Nanofabrication Facility of the CUNY Advanced Science Research Center (ASRC) for instrument use and scientific and technical assistance, and the staff of the MPBT (physical properties—low temperature) platform of Sorbonne Université for their support. We also acknowledge Professors D. J. Smith and M. McCartney at Arizona State University for STEM images.

AUTHOR DECLARATIONS

Conflict of Interest

The authors have no conflicts to disclose.

Author Contributions

Candice R. Forrester: Conceptualization (equal); Data curation (lead); Formal analysis (lead); Writing – original draft (equal). **Christophe Testelin:** Conceptualization (equal); Data curation (supporting); Formal analysis (supporting); Writing – original draft (equal). **Kaushini Wickramasinghe:** Data curation (supporting); Writing – original draft (supporting). **Ido Levy:** Conceptualization (supporting); Data curation (supporting); Writing – original draft (supporting). **Dominique Demaille:** Data curation (supporting). **David Hrabovsky:** Data curation (supporting). **Xiaxin Ding:**

Data curation (supporting). **Lia Krusin-Elbaum**: Conceptualization (equal); Writing – original draft (supporting). **Gustavo E. Lopez**: Conceptualization (supporting). **María C. Tamargo**: Conceptualization (equal); Formal analysis (supporting); Funding acquisition (lead); Project administration (lead); Writing – original draft (equal).

DATA AVAILABILITY

The data that support the findings of this study are available from the corresponding author upon reasonable request.

REFERENCES

- T. Fujita, M. B. A. Jalil, and S. G. Tan, “Topological insulator cell for memory and magnetic sensor applications,” *Appl. Phys. Express* **4**(9), 094201 (2011).
- A. Y. Kitaev, “Fault-tolerant quantum computation by anyons,” *Ann. Phys.* **303**(1), 2–30 (2003).
- A. Stern and N. H. Lindner, “Topological quantum computation—From basic concepts to first experiments,” *Science* **339**(6124), 1179–1184 (2013).
- F. D. M. Haldane, “Model for a quantum Hall effect without Landau levels: Condensed-matter realization of the ‘parity anomaly,’” *Phys. Rev. Lett.* **61**(18), 2015–2018 (1988).
- Y. Xia, D. Qian, D. Hsieh, L. Wray, A. Pal, H. Lin, A. Bansil, D. Grauer, Y. S. Hor, R. J. Cava, and M. Z. Hasan, “Observation of a large-gap topological-insulator class with a single Dirac cone on the surface,” *Nat. Phys.* **5**(6), 398–402 (2009).
- H. Zhang, C.-X. Liu, X.-L. Qi, X. Dai, Z. Fang, and S.-C. Zhang, “Topological insulators in Bi_2Se_3 , Bi_2Te_3 and Sb_2Te_3 with a single Dirac cone on the surface,” *Nat. Phys.* **5**(6), 438–442 (2009).
- C. L. Kane and E. J. Mele, “ \mathbb{Z}_2 topological order and the quantum spin Hall effect,” *Phys. Rev. Lett.* **95**(14), 146802 (2005).
- M. He, H. Sun, and Q. L. He, “Topological insulator: Spintronics and quantum computations,” *Front. Phys.* **14**(4), 43401 (2019).
- L. Fu, C. L. Kane, and E. J. Mele, “Topological insulators in three dimensions,” *Phys. Rev. Lett.* **98**(10), 106803 (2007).
- S. Nakajima, “The crystal structure of $\text{Bi}_2\text{Te}_{3-x}\text{Se}_x$,” *J. Phys. Chem. Solids* **24**(3), 479–485 (1963).
- T. L. Anderson and H. B. Krause, “Refinement of the Sb_2Te_3 and $\text{Sb}_2\text{Te}_2\text{Se}$ structures and their relationship to nonstoichiometric $\text{Sb}_2\text{Te}_{3-y}\text{Se}_y$ compounds,” *Acta Crystallogr., Sect. B: Struct. Crystallogr. Cryst. Chem.* **30**(5), 1307–1310 (1974).
- J. A. Hagmann, X. Li, S. Chowdhury, S.-N. Dong, S. Rouvimov, S. J. Pookpanratana, K. M. Yu, T. A. Orlova, T. B. Bolin, C. U. Segre, D. G. Seiler, C. A. Richter, X. Liu, M. Dobrowolska, and J. K. Furdyna, “Molecular beam epitaxy growth and structure of self-assembled $\text{Bi}_2\text{Se}_3/\text{Bi}_2\text{MnSe}_4$ multilayer heterostructures,” *New J. Phys.* **19**(8), 085002 (2017).
- C.-X. Liu, S.-C. Zhang, and X.-L. Qi, “The quantum anomalous Hall effect: Theory and experiment,” *Annu. Rev. Condens. Matter Phys.* **7**, 301–321 (2016).
- C. Z. Chang, J. Zhang, X. Feng, J. Shen, Z. Zhang, M. Guo, K. Li, Y. Ou, P. Wei, L. L. Wang, Z. Q. Ji, Y. Feng, S. Ji, X. Chen, J. Jia, X. Dai, Z. Fang, S. C. Zhang, K. He, Y. Wang, L. Lu, X. C. Ma, and Q. K. Xue, “Experimental observation of the quantum anomalous Hall effect in a magnetic topological insulator,” *Science* **340**(6129), 167–170 (2013).
- X. Kou, Y. Fan, M. Lang, P. Upadhyaya, and K. L. Wang, “Magnetic topological insulators and quantum anomalous Hall effect,” *Solid State Commun.* **215–216**, 34–53 (2015).
- T. Murakami, Y. Nambu, T. Koretsune, G. Xiangyu, T. Yamamoto, C. Brown, and H. Kageyama, “Realization of interlayer ferromagnetic interaction in MnSb_2Te_4 toward the magnetic Weyl semimetal state,” *Phys. Rev. B* **100**(19), 195103 (2019).
- E. D. L. Rienks, S. Wimmer, J. Sánchez-Barriga, O. Caha, P. S. Mandal, J. Růžička, A. Ney, H. Steiner, V. V. Volobuev, H. Groiss, M. Albu, G. Kothleitner, J. Michalička, S. A. Khan, J. Minár, H. Ebert, G. Bauer, F. Freyse, A. Varykhalov, O. Rader, and G. Springholz, “Large magnetic gap at the Dirac point in $\text{Bi}_2\text{Te}_3/\text{MnBi}_2\text{Te}_4$ heterostructures,” *Nature* **576**(7787), 423–428 (2019).
- Y. Tokura, K. Yasuda, and A. Tsukazaki, “Magnetic topological insulators,” *Nat. Rev. Phys.* **1**(2), 126–143 (2019).
- S. Wimmer, J. Sánchez-Barriga, P. Küppers, A. Ney, E. Schierle, F. Freyse, O. Caha, J. Michalička, M. Liebmann, D. Primetzhofer, M. Hoffman, A. Ernst, M. M. Otrokov, G. Bihlmayer, E. Weschke, B. Lake, E. V. Chulkov, M. Morgenstern, G. Bauer, G. Springholz, and O. Rader, “Mn-rich MnSb_2Te_4 : A topological insulator with magnetic gap closing at high Curie temperatures of 45–50 K,” *Adv. Mater.* **33**(42), 2102935 (2021).
- H. Zhang, W. Yang, Y. Wang, and X. Xu, “Tunable topological states in layered magnetic materials of MnSb_2Te_4 , MnBi_2Se_4 , MnSb_2Se_4 ,” *Phys. Rev. B* **103**(9), 094433 (2021).
- S. Huan, S. Zhang, Z. Jiang, H. Su, H. Wang, X. Zhang, Y. Yang, Z. Liu, X. Wang, N. Yu, Z. Zou, D. Shen, J. Liu, and Y. Guo, “Multiple magnetic topological phases in bulk van der Waals crystal MnSb_4Te_7 ,” *Phys. Rev. Lett.* **126**(24), 246601 (2021).
- A. N. Tamanna, A. Lakra, X. Ding, E. Buzi, K. Park, K. Sobczak, H. Deng, G. Sharma, S. Tewari, and L. Krusin-Elbaum, “Hydrogen induces chiral conduction channels in the topological magnet,” [arXiv:2312.02315](https://arxiv.org/abs/2312.02315) (2023).
- S.-Y. Xu, I. Belopolski, N. Alidoust, M. Neupane, G. Bian, C. Zhang, R. Sankar, G. Chang, Z. Yuan, C.-C. Lee, S.-M. Huang, H. Zheng, J. Ma, D. S. Sanchez, B. Wang, A. Bansil, F. Chou, P. P. Shibayev, H. Lin, S. Jia, and M. Z. Hasan, “Discovery of a Weyl fermion semimetal and topological Fermi arcs,” *Science* **349**(6248), 613–617 (2015).
- C. Guo, V. Asadchy, B. Zhao, and S. Fan, “Light control with Weyl semimetals,” *eLight* **3**, 2 (2023).
- H. Deng, Z. Chen, A. Wołoś, M. Konczykowski, K. Sobczak, J. Sitnicka, I. V. Fedorchenko, J. Borysiuk, T. Heider, Ł. Pluciński, K. Park, A. B. Georgescu, J. Cano, and L. Krusin-Elbaum, “High-temperature quantum anomalous Hall regime in a $\text{MnBi}_2\text{Te}_4/\text{Bi}_2\text{Te}_3$ superlattice,” *Nat. Phys.* **17**(1), 36–42 (2021).
- Y. Deng, Y. Yu, M. Z. Shi, Z. Guo, Z. Xu, J. Wang, X. H. Chen, and Y. Zhang, “Quantum anomalous Hall effect in intrinsic magnetic topological insulator MnBi_2Te_4 ,” *Science* **367**(6480), 895–900 (2020).
- Y. Liu, L.-L. Wang, Q. Zheng, Z. Huang, X. Wang, M. Chi, Y. Wu, B. C. Chakoumakos, M. A. McGuire, B. C. Sales, W. Wu, and J. Yan, “Site mixing for engineering magnetic topological insulators,” *Phys. Rev. X* **11**(2), 021033 (2021).
- I. Levy, C. Forrester, X. Ding, C. Testelin, L. Krusin-Elbaum, and M. C. Tamargo, “High Curie temperature ferromagnetic structures of $(\text{Sb}_2\text{Te}_3)_{1-x}(\text{MnSb}_2\text{Te}_4)_x$ with $x = 0.7\text{--}0.8$,” *Sci. Rep.* **13**(1), 7381 (2023).
- I. Levy, C. Forrester, H. Deng, M. Roldan-Gutierrez, M. R. McCartney, D. J. Smith, C. Testelin, L. Krusin-Elbaum, and M. C. Tamargo, “Compositional control and optimization of molecular beam epitaxial growth of $(\text{Sb}_2\text{Te}_3)_{1-x}(\text{MnSb}_2\text{Te}_4)_x$ magnetic topological insulators,” *Cryst. Growth Des.* **22**(5), 3007–3015 (2022).
- D. S. Lee, T.-H. Kim, C.-H. Park, C.-Y. Chung, Y. S. Lim, W.-S. Seo, and H.-H. Park, “Crystal structure, properties and nanostructuring of a new layered chalcogenide semiconductor, Bi_2MnTe_4 ,” *CrystEngComm* **15**(27), 5532–5538 (2013).
- Z. Zhou, Y.-J. Chien, and C. Uher, “Thin-film ferromagnetic semiconductors based on $\text{Sb}_{2-x}\text{V}_x\text{Te}_3$ with T_C of 177 K,” *Appl. Phys. Lett.* **87**(11), 112503 (2005).
- Z. Zhou, Y.-J. Chien, and C. Uher, “Thin film dilute ferromagnetic semiconductors $\text{Sb}_{2-x}\text{Cr}_x\text{Te}_3$ with a Curie temperature up to 190 K,” *Phys. Rev. B* **74**(22), 224418 (2006).
- M. G. Vergniory, M. M. Otrokov, D. Thonig, M. Hoffmann, I. V. Maznichenko, M. Geilhufe, X. Zubizarreta, S. Ostanin, A. Marmorodo, J. Henk, W. Hergert, I. Mertig, E. V. Chulkov, and A. Ernst, “Exchange interaction and its tuning in magnetic binary chalcogenides,” *Phys. Rev. B* **89**(16), 165202 (2014).
- K. Sumida, Y. Ishida, J. Gütde, U. Höfer, S. Shin, and A. Kimura, “Ultrafast surface Dirac fermion dynamics of Sb_2Te_3 -based topological insulators,” *Prog. Surf. Sci.* **96**(2), 100628 (2021).
- M. F. Islam, C. M. Canali, A. Pertsova, A. Balatsky, S. K. Mahatha, C. Carbone, A. Barla, K. A. Kokh, O. E. Tereshchenko, E. Jiménez, N. B. Brookes, P. Gargiani, M. Valvidares, S. Schatz, T. R. F. Peixoto, H. Bentmann, F. Reinert, J. Jung, T. Bathon, K. Fauth, M. Bode, and P. Sessi, “Systematics of electronic and magnetic properties in the transition metal doped Sb_2Te_3 quantum anomalous Hall platform,” *Phys. Rev. B* **97**(15), 155429 (2018).

- ³⁶J.-Q. Yan, S. Okamoto, M. A. McGuire, A. F. May, R. J. McQueeney, and B. C. Sales, "Evolution of structural, magnetic, and transport properties in $\text{MnBi}_{2-x}\text{Sb}_x\text{Te}_4$," *Phys. Rev. B* **100**(10), 104409 (2019).
- ³⁷Y. Chen, Y. W. Chuang, S. H. Lee, Y. Zhu, K. Honz, Y. Guan, Y. Wang, K. Wang, Z. Mao, J. Zhu, C. Heikes, P. Quarterman, P. Zajdel, J. A. Borchers, and W. Ratcliff, "Ferromagnetism in van der Waals compound $\text{MnSb}_{1.8}\text{Bi}_{0.2}\text{Te}_4$," *Phys. Rev. Mater.* **4**(6), 064411 (2020).
- ³⁸D. Kong, Y. Chen, J. J. Cha, Q. Zhang, J. G. Analytis, K. Lai, Z. Liu, S. S. Hong, K. J. Koski, S.-K. Mo, Z. Hussain, I. R. Fisher, Z.-X. Shen, and Y. Cui, "Ambipolar field effect in the ternary topological insulator $(\text{Bi}_x\text{Sb}_{1-x})_2\text{Te}_3$ by composition tuning," *Nat. Nanotech.* **6**(11), 705–709 (2011).
- ³⁹R. Akiyama, K. Sumida, S. Ichinokura, R. Nakanishi, A. Kimura, K. A. Koh, O. E. Tereshchenko, and S. Hasegawa, "Shubnikov-de Haas oscillations in *p* and *n*-type topological insulator $(\text{Bi}_x\text{Sb}_{1-x})_2\text{Te}_3$," *J. Phys.: Condens. Matter* **30**(26), 265001 (2018).
- ⁴⁰T. Kasuya, "A theory of metallic ferro- and antiferromagnetism on Zener's model," *Prog. Theor. Phys.* **16**(1), 45–57 (1956).
- ⁴¹M. A. Ruderman and C. Kittel, "Indirect exchange coupling of nuclear magnetic moments by conduction electrons," *Phys. Rev.* **96**(1), 99–102 (1954).
- ⁴²K. Yosida, "Anomalous electrical resistivity and magnetoresistance due to an *s*-*d* interaction in Cu–Mn alloys," *Phys. Rev.* **107**(2), 396–403 (1957).
- ⁴³J. H. Van Vleck, "Models of exchange coupling in ferromagnetic media," *Rev. Mod. Phys.* **25**(1), 220–227 (1953).
- ⁴⁴F. Wang, Y.-F. Zhao, Z.-J. Yan, D. Zhuo, H. Yi, W. Yuan, L. Zhou, W. Zhao, M. H. W. Chan, and C.-Z. Chang, "Evolution of dopant-concentration-induced magnetic exchange interaction in topological insulator thin films," *Nano Lett.* **23**(7), 2483–2489 (2023).
- ⁴⁵R. Yu, W. Zhang, H.-J. Zhang, S.-C. Zhang, X. Dai, and Z. Fang, "Quantized anomalous Hall effect in magnetic topological insulators," *Science* **329**(5987), 61–64 (2010).